Investigation on the mechanical interface stability of curved high aspect ratio x-ray gratings made by deep x-ray lithography

Michael Richter,[a] Thomas Beckenbach,[b] Heiner Daerr,[c] Sven Prevrhal,[c] Martin Börner,[a,d] Josephine Gutekunst,[a] Pouria Zangi,[a] Arndt Last,[a,d] Jan G. Korvink,[a] and Pascal Meyer[a,*]

[a]Karlsruhe Institute of Technology, Institute of Microstructure Technology, Eggenstein-Leopoldshafen, Germany
[b]microworks GmbH, Karlsruhe, Germany
[c]Philips GmbH Innovative Technologies, Research Laboratories Hamburg, Hamburg, Germany
[d]KNMFi, Eggenstein-Leopoldshafen, Germany

Abstract. We describe the rationale for selecting graphite as a substrate material suitable for manufacturing curved high-aspect ratio metallic x-ray gratings and experimentally validate that its properties satisfy requirements relevant for clinical phase-contrast and dark-field x-ray imaging. Selection criteria applied to two candidate materials graphite and polyimide were compliance to bending, mechanical tenacity of the attachment of the lamellar grating structure to the substrate, the substrate material's x-ray robustness, and the compatibility with the x-ray LIGA process used to manufacture the grating structures. In contrast to other standard materials such as silicon wafers with titanium layer, graphite wafers could be bent to smaller radii and are natively electrically conductive. While polyimide wafers allowed for even smaller bending radii, we found their high risk of grating structure detachment to be a strong detractor. Minimum achievable bending radii were 55 and 70 mm for pure graphite wafers and graphite wafers with mounted grating structure, respectively. Electron microscopy of graphite surface and cross-sections revealed a fine porous structure conducting to a very stable metal–wafer interface. Grating structures with heights of more than 200 μm were bonded to graphite wafers and their integrity confirmed in flat as well as in bent state using microfocus x-ray imaging. We conclude that graphite is a very well-suited substrate material for manufacturing curved x-ray gratings. [DOI: 10.1117/1.JMM.21.2.024901]

Keywords: x-ray gratings; deep x-ray lithography; graphite wafers.

Paper 22009G received Feb. 22, 2022; accepted for publication May 5, 2022; published online May 25, 2022.

1 Introduction

Clinical diagnostic x-ray imaging is currently based on the principle of differences of x-ray attenuation between tissues. Whereas attenuation contrast is often insufficient to allow differentiation between tissues such as cancer lesions in soft tissue or pathologic changes in the lung, research points to phase-contrast, and dark-field x-ray imaging as an option to overcome this limitation, with clinical[1–5] as well as industrial applicability.[6] Currently, the most promising technology to do phase contrast and dark-field imaging is interferometry using a Talbot–Lau interferometer, which requires microstructured gratings.[7,8]

In this technique, differential changes to the x-ray phase induced by the tissues or materials passed through by the x-ray beam are transferred to an intensity pattern that can then be detected by a conventional x-ray detector. Three x-ray optics microstructure gratings are needed for a Talbot–Lau interferometer. The first grating (source grating) is located close to the x-ray source

*Address all correspondence to Pascal Meyer, pascal.meyer@kit.edu

and creates spatial coherence of the radiation emitted by the source. The second grating (phase grating) periodically shifts the phase of passing x-rays, resulting in a so-called Talbot pattern behind this grating, with the property that at a certain distance (fractional Talbot distance) the grating maps into a periodic intensity pattern. Since the period of the pattern is in the range of a few micrometers, but conventional x-ray detectors have pixels of 100 μm $\times$ 100 μm or more, a third grating (analyzer grating) is needed with a period matching that of the Talbot pattern. The periods of the gratings are in the range of a few micrometers. The x-rays used range from a few 10 to over 100 keV, depending on the application. For lung screening or computer tomography, the energies should be well above 60 keV. The attenuating lamellae of both the source and analyzer grating need to be sufficiently x-ray opaque. Even with the most strongly attenuating materials with usable mechanical properties, a grating height of several hundred micrometers is required to achieve suitable opacity. The resulting aspect ratio of more than 100 places high demands on the production technology of the microengineered gratings. An additional boundary condition is that the gratings are used in a setup with a conically radiating x-ray tube. A high-aspect ratio grating close to the tube will therefore cause x-ray shadowing outside a very small field of view at the beam center unless the grating lamellae are focused onto the x-ray focus point [Fig. 1(a)]. Such high-aspect ratio x-ray gratings can be produced by x-ray lithography,[9] deep reactive ion etching,[10,11] or by metal assisted chemical etching.[12] All of these processes are performed on flat substrate. To avoid shadowing effects, several solutions exist [Figs. 1(b)–(d)]: on a flat substrate, each grating lamella are inclined as a function of the x-ray incidence angle [Fig. 1(b)]; on a flat substrate, lamellae direction follows the needed radius of curvature [Fig. 1(c)]; the flat substrate with the lamellae is bent to the desired radius of curvature [Fig. 1(d)]. Concerning the first solution, a recent study demonstrates the fabrication of fan-shaped source gratings by modulating the electric field during the deep reactive ion etching of silicon.[13,14] Our fabrication process being the x-ray lithography, this could be performed using

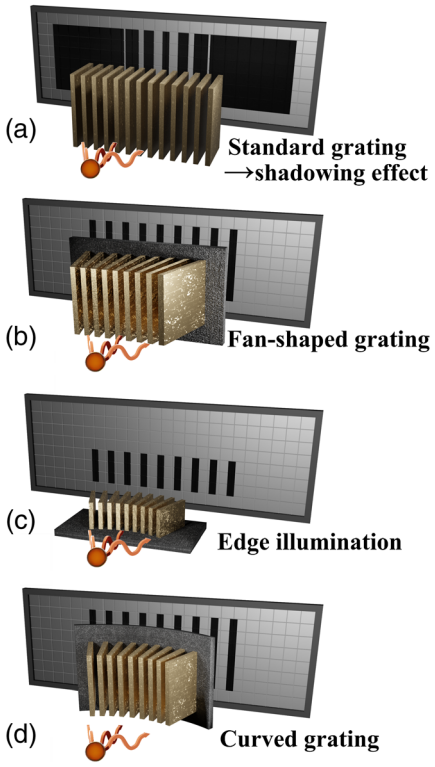

Fig. 1 (a) Shadowing effect with a cone beam x-ray source. (b) On a flat substrate, the lamellae are inclined as a function of the x-ray incidence angle (fan-shaped grating). (c) On a flat substrate, the lamellae direction follows the needed radius of curvature (edge illumination). (d) The substrate, together with the grating lamellae, is bent with the radius corresponding to the placement distance.

an x-ray source (cone beam); in this case, the working mask with higher absorber should be manufactured using this technique. For such processes, studies are ongoing.[15] The second method can already utilize the full precision of the current state-of-the-art lithographic process.[16] However, only a very limited field of view in the vertical direction can be achieved which corresponds to the lamellae height (only some few 100 μm). In this article, focus is placed on the third method where the x-ray grating is made on a flat substrate and subsequently bent to the desired radius. Especially for the source grating, which has a distance of only a few centimeters to the focal spot of the x-ray tube, this is challenging. In addition, the proximity to the tube also places a high thermal load on the grating, leading to strong temperature fluctuations during operation. Furthermore, the x-ray exposure itself may lead to material changes over time. To ensure a reliable commercial use of the process, it must be guaranteed that the grating can withstand these stresses for years (desirably 10 years). The described gratings are currently fabricated using the direct deep x-ray LIGA process: x-ray deep lithography and electroplating in gold. Usually, the polymer (also referred to as resist) remains after electroplating to ensure sufficient stability of the fine metal walls. The standard substrate used is a silicon wafer with a titanium coating. Previous investigations have shown that 200- or 550-μm thick silicon breaks when bent with a radius of around 10 cm and is therefore not suitable as a substrate. The first orientating tests showed that carbon or substrates made of x-ray resistant polymer can be used for this purpose.[17] However, even if an x-ray resist is used as the mold for electroplating, it is known that the plastic degrades and becomes more brittle with increasing radiation exposure. Since it must be assumed that the degradation will lead to a change in the x-ray optical behavior of the grating structures and a deterioration of the image quality, it will probably not be advisable to leave the plastic inside the structure. Removal is affected by a plasma process called stripping.

Further investigation was necessary to show whether the metallic grating lamellae with their base width of a few micrometers maintain their adherence to the substrate in the interface under bending stress. In addition to the bending stress, the removal of resist is of concern for the mechanical stability. Since it can be surmised that the quality of the interface between metallic lamellae and the substrate is decisive for adhesion, mechanical interlocking could be advantageous compared with a purely chemical bond. In the following, we present an SWOT analysis (strengths, weaknesses, opportunities, and threats) of the otherwise suitable substrate types. For the strongest contender, the bending limits, materials porosity, and the interface between the metal lamellae and the substrate are studied. In the following, the gratings used are "bridge" type; a small photoresist area (the bridge, 1 to 2 μm long) connects photoresist lamellae for improved mechanical stability also during the electroplating step. Consequently, these regions will not be electroplated and thus represent openings in the final grating state, when the resist is removed. Results of corresponding experimental tests are presented for a source grating with a period of 7.72 μm source grating with a bending radius of 12 cm are presented.

2 Selection of Substrate Material

Concerning the deep x-ray LIGA process, 525 μm silicon 4-in. wafers with a coated metallic layer (either with 2.5 μm titanium, or a few 10 nm Cr/Au) are typically used. They have very limited potential for bending, as they will break already for large radii. By reducing the thickness to 200 μm, or even to 100 μm, the bending capability increases, but at the expense of robustness. They are extremely fragile and very often break during the fabrication process. Other candidates are polyimide and graphite wafers; an SWOT analysis comparing graphite and polyimide is presented in Table 1, where the three first lines indicate their properties in terms of thickness, x-ray attenuation, and conductivity (is a conductive layer needed or not? and if yes which one). The threats of both materials are comparable in severity in the sense that realization of either threat would render the grating unusable. With respect to opportunities, the radii that can be achieved with polyimide are smaller than those for graphite, which opens the opportunity for a wider range of applications. However, in view of fully stripped grating, the weakness of polyimide concerning the structure adhesion problem and its deterioration during plasma etching is rated more severely toward the threat of grating destruction. Thus, graphite is chosen here as the preferable substrate material.

Table 1 X-ray lithography: SWOT analysis for substrates.

	Graphite	Polyimide
Thickness	200, 500, 1000 μm	500 and 1000 μm
X-ray attenuation	Low	Low
Conductive layer	None	CrAu, conductive lack
Strength	Bendable, rough surface, conductive, very strong interface, no additional dose by secondary radiation[18]	Very bendable, very small radii in principle
Weakness	Inhomogeneous and porous which leads to resist spin coating problems and can make production challenging	Not conductive; need sputtering steps, or conductive lack. No strong adhesion of conductive layer. Polyimide will be deteriorated by plasma etching resist removal
Opportunities	Superior durability leading to lower maintenance effort	Wider range of applications
Threats	Destruction due to breaking for small radii and/or defects in the material	Detachment of the conductive layer and destruction due to loss of adhesion to the structure

2.1 *Analysis of the Substrate/Grating—Method Used*

First, the mechanical stability of the chosen substrate material was tested. Measurements to establish bending limits were carried out using a four point flexural test setup according to DIN EN 843-115[19] on a Texture Analyzer (TA.XTplus, Stable Micro Systems, Godalming, Surrey, United Kingdom) with a custom-made bending head (Fig. 2). As graphite is a brittle material and cannot be expected to be very homogeneous, this method was chosen over a three-point bending setup to distribute the stress more homogeneously over the sample length.

Studies on the materials porosity and the interface between the metal lamellae and the substrate were performed using cross-sections of the respective parts. For the cross-sections, an JEOL Ion Beam Cross Section Polisher (CP) was used (JEOL, Peabody, Massachusetts). Inspection of the cross-sections was carried out using a Zeiss Supra scanning electron microscope. All high aspect-ratio test grating samples were fabricated using the state-of-the-art x-ray LIG(A) technique; the exposures were performed at the KIT synchrotron facility KARA.

The x-ray properties of the gratings were investigated using a simple x-ray transmission setup comprising of a microfocus x-ray tube with output power-dependent focal size of 6 to 100 μm (Kevex PXS1065W, Thermo Fisher Scientific, Scotts Valley, California), sample holder, and an x-ray detector with an active area of 100×50 mm^2 and a pixel pitch of 48 μm (Shad-o-Box 2048 EV, Rad-icon, Santa Clara, California) (Fig. 3).

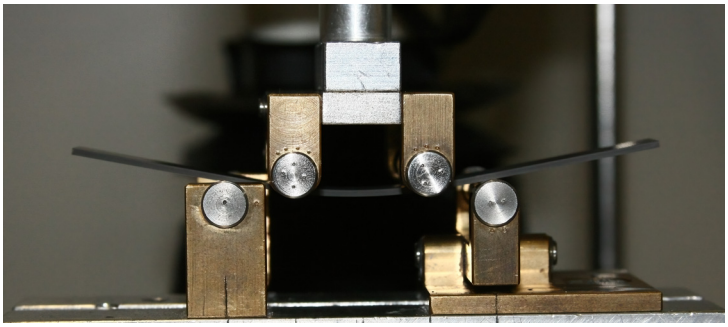

Fig. 2 Custom head for the four-point bending process. The two inner pressure points have a distance of 2 cm. The two outer pressure points have a distance of 4 cm. The pressure rolls are movable and allow for an even placement of the sample.

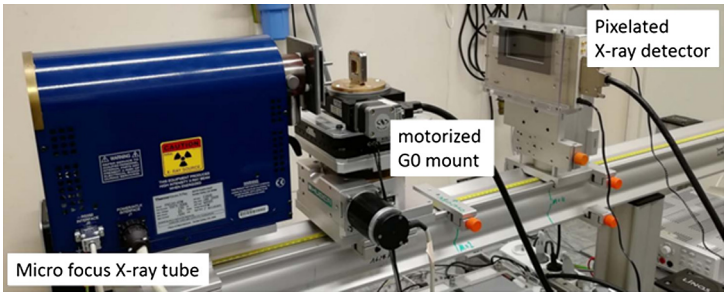

Fig. 3 X-ray test setup.

Measurements of the gratings in flat and bent states were carried out at tube voltages ranging from 20 to 130 kVp and up to 500 μA tube current. An additional tube-side filtration of 1 mm aluminum was used.

2.2 *Graphite Properties*

Graphite as a material offers a variety of the desired properties for source gratings. It is highly transparent for x-rays and is bendable. Further, depending on the grain size, graphite has a fine porous structure with a rough surface ideal for achieving a strong adhesion of the grating lamellae as these can be mechanically linked into the surface. In addition, graphite is a natural conductor. Therefore, a conductive coating layer for the electroplating step is not needed. For this work, the EDM-AF5 grade carbon (OCB) was used.[20] This type of graphite promises an average grain size of 1 μm, a flexural strength of 100 MPa, and is available in various sizes and custom shapes. Four-inch wafers with thicknesses of 1000, 500, and 200 μm were used. Thickness variations were specified to be within 20 for 1000 μm and 15 μm for 500 and 200 μm, respectively. Electron microscopy of the bare-material cross-sections revealed that indeed the material had a very fine structure with visible grains in the order of 1 μm. The distribution homogeneity of the pores with sizes between 2 and 5 μm was found to be very even, thus promoting sufficient penetration of the resist layer into the substrate surface during grating production [Fig. 5(a)].

2.2.1 *Bending*

To investigate the limits of bending of the graphite type, the four-point bending setup was used till the breaking point with slices of different wafers. For all thicknesses, initially a set of 10 samples for each thickness was used from the wafers center that would normally be housing the grating. Each sample was then bent with the minimal possible speed of 0.1 mm per second in a continuous mode. The results are presented in Table 2. The 10×200 μm samples, however, could not be bent meaningfully as their breaking point is found to be lower than the minimal radius of 2 cm from the four-point bending head. At this point, it is necessary to note that it turned out during the grating production that the 200 μm graphite wafers are actually too flexible for high aspect ratio grating. The thin graphite deforms greatly in the process due to resist shrinkage of the photo resist layer. Therefore, these wafers were excluded in all further investigations.

Table 2 Minimal mean radii for bend graphite stripes. All results are way below 10 cm. The maximum radius indicates the extreme value that was found during the measurement and is an estimation of the upper limit.

Graphite thickness (μm)	Mean flexural strength (MPa)	Mean radius (cm)	Maximum radius (cm)
1000 ± 20	120.5 ± 5.8	5.6 ± 0.3	6.9 ± 0.47
500 ± 15	105.5 ± 5.6	5.1 ± 0.23	6.5 ± 0.4
200 ± 15	—	≤ 2	≤ 2

The measured values for flexural strength of 500 μm wafer are in good agreement with the claims of the supplier, while the value for 1000 μm being 20% larger. This gives the emphasis in using the 500 μm wafer for grating production.

To test the bending limits with the grating lamellae, the same bending process as before was applied to two gratings (graphite thickness 500 μm). The heights of these gratings after production were 150 μm with a lamella width of 2.4 μm and a duty cycle of 0.5 (period is 4.8 μm). The test was conducted in unstripped as well as in stripped state. In this experiment, bending was performed in stepwise fashion to detect potential early detachment. This setup allows for a flexible investigation of the bent area. During bending, detachment was not observed; some distorted lamellae at the outer edges were present but as a result of resist stripping [Fig. 4(a)]. The resulting final radii, presented in Table 3, are only slightly larger than the previously established values for the pure graphite and well below 10 cm.

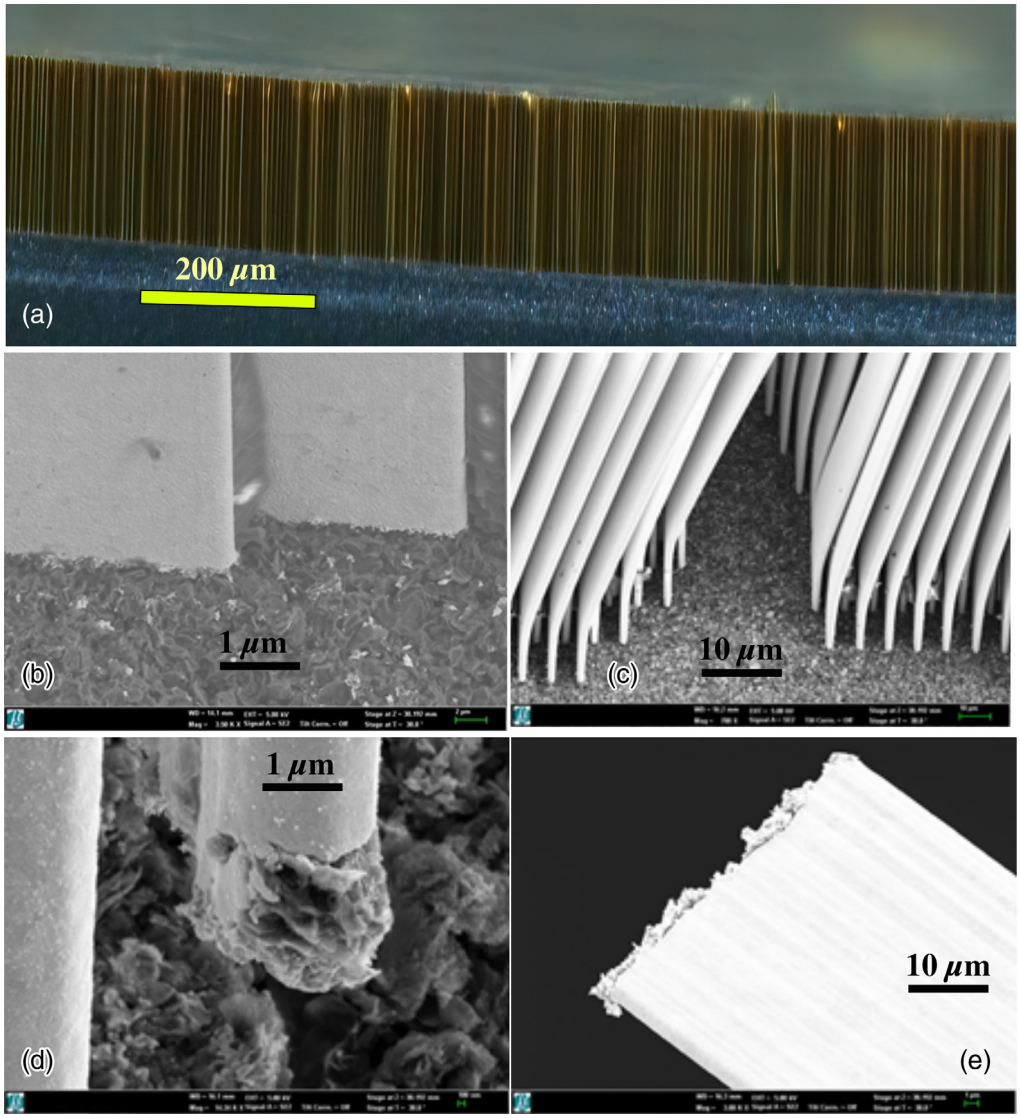

Fig. 4 (a) Bent stripped x-ray grating. Only single lamellae at the outer edges are deformed. No visible detachment is occurring. (b) Interface of the unstripped sample close to the breaking edge. The grating lamellae are overall well attached to the graphite surface. (c) Lamellae graphite interface for stripped grating after bending till the breaking point. The lamellae are tilted in the direction of the breaking edge but are almost entirely attached to the graphite surface. (d) Partially lifted lamella. The lamella base is entirely connected to graphite broken of the surface. (e) Completely broken out lamella. The lamella has a thick layer of graphite attached to its base that is broken out of the graphite bulk.

Table 3 Minimal bending radii for x-ray gratings (graphite thickness 500 μm). Both results are below 10 cm.

Breaking radius (resist stripped) (cm)	Breaking radius (resist nonstripped) (cm)
6.0 ± 0.4	7.1 ± 0.4

Both samples were inspected afterward with SEM. The unstripped sample was found to have no further detachment [Fig. 4(b)] except in the immediate surrounding of the breaking edge. The stripped sample, on the other hand, exhibited lamellae distortion in the direction of the breaking force as expected. However, the interface was found almost entirely intact, and the lamellae were still connected to the surface [Fig. 4(c)]. In case of partially or fully detached lamellae, grains of graphite were found broken out alongside and were tightly attached to the bottom end of the lamellar structure [Figs. 4(d) and 4(e)]. From the cross-section studies, the interface is here already known to be deeply interconnected. Therefore, this can be interpreted as a breaking of the graphite bulk. In this case, the limiting factor for the grating concerned the mechanical stability of the graphite.

2.2.2 *Interface*

When this graphite type was used in actual grating production, no additional layer was placed between the lamellae and the wafer material, and the resulting interface could be inspected on a

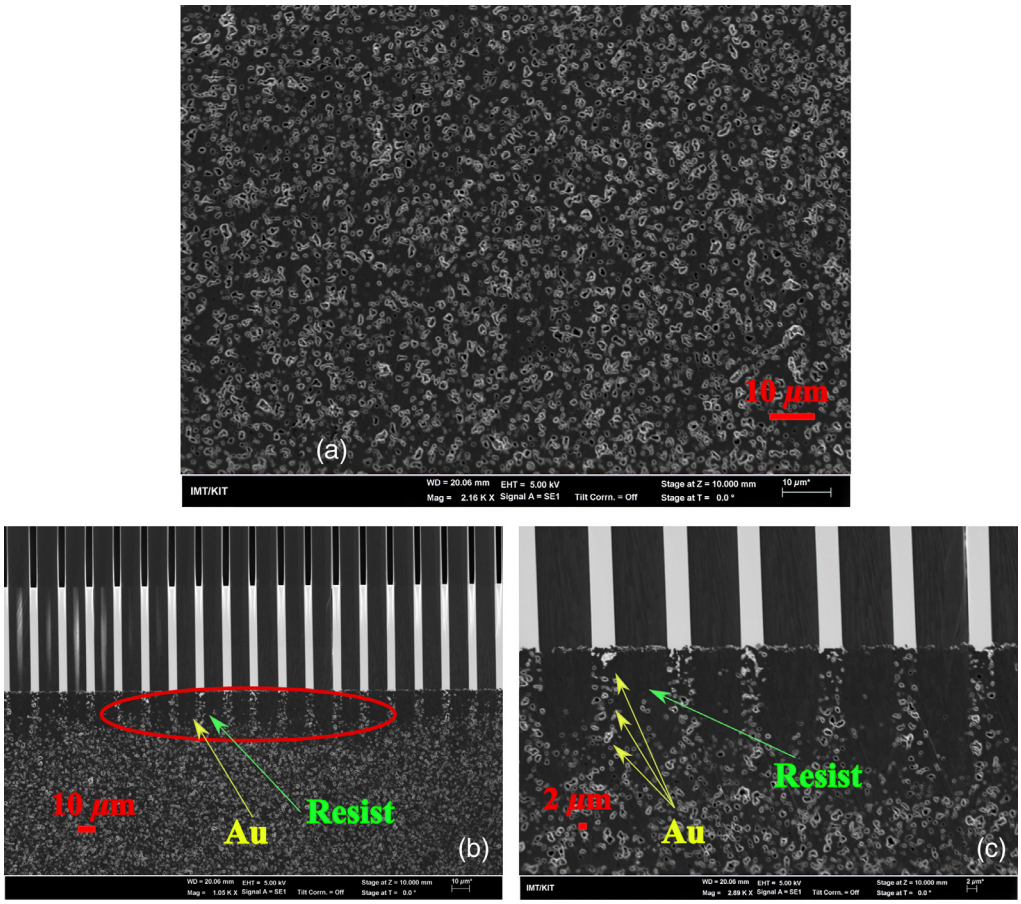

Fig. 5 Electron microscopy images of the cross-section of graphite AF5 OCB. (a) A fine homogeneous porous structure is present. The overall grain size was found to be in the order of 1 μm, with pore sizes between 2 and 5 μm. (b) Interface cross-section (red oval mark). (c) Magnification of (b): the black bars inside the graphite bulk indicate the resist penetration. The gold brighter spots inside the pores indicate the deepness of the lamellae base.

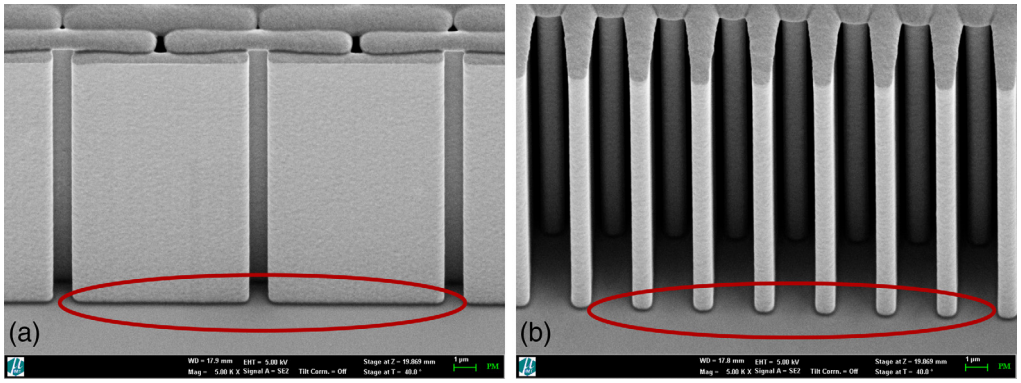

Fig. 6 (a) and (b) Metal lamellae on metal coated polyimide surface. In contrast to graphite, the interface (red oval mark) is not anchored into the surface. The resist is removed.

polished cross-section. The interface proved to be very strong as the metal lamellae and the surrounding resist structure were embedded into the surface to a depth of at least 5 and 10 μm, respectively [Figs. 5(b), and 5(c)]. In contrast, the same deep interconnection could not be achieved with a polyimide substrate as no porous structure is present. The lamellae stood directly on the very thin conductive surface layer [Figs. 6(a) and 6(b)].

3 X-Ray Imaging of Gratings

A source grating with an area of 2.1×2.1 cm^2, period of 7.72 μm, duty cycle 0.7, and a gold absorption thickness of 220 μm was designed. The source grating was placed near the source, with a bending radius of 12 cm. The sample was first imaged in a flat state [Fig. 7(b)] and afterward carefully placed in a stainless-steel bending holder with 12 cm bending radius [Fig. 7(a)]; the lamellae were pointing toward the bending radius center [Fig. 7(c)]. After the measurements in the unstripped state, the resist was removed and the sample measured again. Figure 8 shows typical results of the experiment. Small errors that can be seen on the flat samples are attributed to defects already present on the mask.

All images were taken at 70 kVp and 200 mA with a focal spot size of about 20 μm. The images are normalized using flat field and dark field. In the flat state and closer to the x-ray source (12 cm), the typical shadowing is present leaving only the center region illuminated [Figs. 8(a) and 8(a′)]. It is already visible that the grating quality is degraded after stripping the resist. This is more visible by increasing the distance x-ray source-grating; the shadowing vanishes but the defects, such as cracks already present in the unstripped state, are more

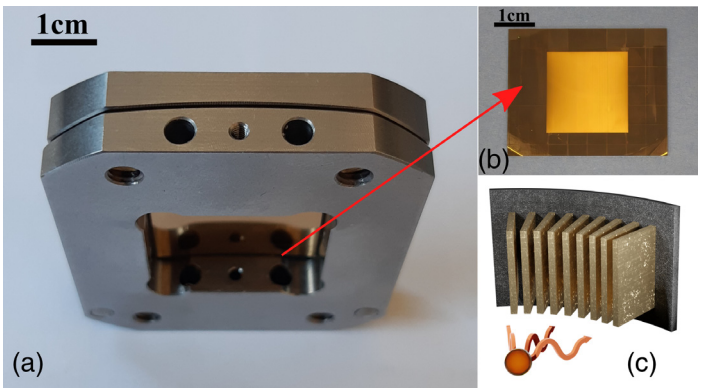

Fig. 7 (a) Stainless-steel bending holder with a radius of curvature of 12 cm at the interface with the lamellae pointing to the center of the radius as shown in the illustration (c). (b) Test grating in flat state. The small vertical lines are errors present already at the fabrication mask.

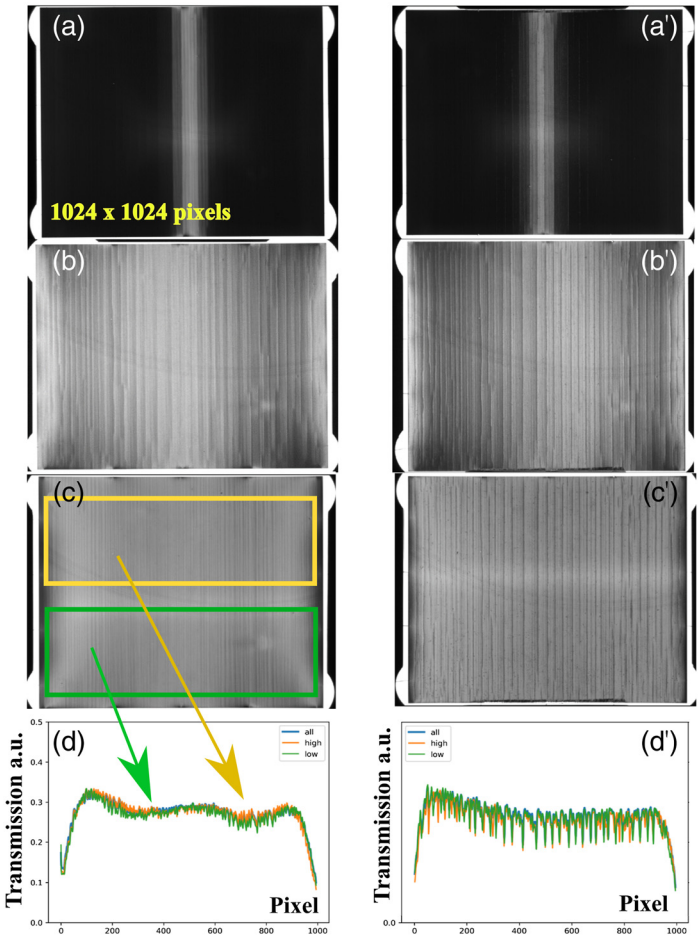

Fig. 8 X-ray images of the substrate-mounted grating. The left side (a to d) corresponds to the grating in a nonstripped state; the right side to the grating with fully removed resist (a′ to d′). (a) and (a′) The grating is flat, the distance grating-x-ray to source is 12 cm. (b) and (b′) The grating is flat, the distance to source is 66 cm. (c) and (c′) The grating is bent with 12 cm radius of curvature, the distance to source is 12 cm. (d) and (d′) Measured transmission profiles of the bent gratings in arbitrary units.

pronounced [Figs. 8(b) and 8(b′)]. By bending the grating corresponding to the 12 cm distance to the x-ray source, the lamellae pointing toward the bending radius center, there is a compression of the resist and lamellae, and the gaps between them (cracks) will be minimized; the grating quality in the bent state increase [Fig. 8(c)]. The transmission is almost constant along the x-axis (axis orthogonal to the lamellae direction), which demonstrates the capability of the grating/substrate to be curved [Fig. 8(d)]. After removing the resist, the cracks visible in the flat state are again present in the curved state [compare Figs. 8(b′) and (c′)]. These results were reproduced using another grating; in all cases, no problems occur concerning the bending of the graphite substrate; the grating x-ray transmission is more homogeneous across the whole grating when the resist is not removed.

4 Conclusion

In summary, we demonstrate the advantages of using graphite as wafer material for the production of bent x-ray gratings. Using 500-μm thick graphite wafers of type AF5 OCB, the maximum curvature (minimum radius of curvature) is <10 cm. Furthermore, the porosity offers a very important anchoring of the structures with the substrate, which is a guarantee of great stability. If the resist is not removed, the quality in terms of x-ray transmission of the curved grating is

even improved. By removing the resist, in view of long-term use to meet industrial requirements, the adhesion of the structure is still good enough, but the overall quality, even if satisfactory for phase contrast imaging, is degraded; our results are hence limited. Currently, we proceed with increasing the structure stability by connecting them with bars.[21]

Acknowledgments

The authors acknowledge the support of the Karlsruhe Nano Micro Facility (KNMFi), the KARA synchrotron light source facility at the Karlsruhe Institute of Technology (KIT) as well as funding from EIT Health. We further acknowledge the support of the Karlsruhe School of Optics and Photonics (KSOP, financed by the Ministry of Science, Research and Arts of Baden-Württemberg as part of the sustainability financing of the projects of the Excellence Initiative II) as well as the support of the KIT-Publication Fund of the Karlsruhe Institute of Technology.

References

1. M. Viermetz et al., "Dark-field computed tomography reaches the human scale," *Proc. Natl. Acad. Sci. U. S. A.* **119**(8), e2118799119 (2022).
2. K. Willer et al., "X-ray dark-field chest imaging for detection and quantification of emphysema in patients with chronic obstructive pulmonary disease: a diagnostic accuracy study," *Lancet Digital Health* **3**(11), e733–e744 (2021).
3. F. Horn et al., "Implementation of a Talbot–Lau interferometer in a clinical-like c-arm setup: a feasibility study," *Sci. Rep.* **8**(1), 2325 (2018).
4. A. Momose, "X-ray phase imaging reaching clinical uses," *Phys. Med.* **79**, 93–102 (2020).
5. C. Arboleda et al., "Towards clinical grating-interferometry mammography," *Eur. Radiol.* **30**(3), 1419–1425 (2020).
6. S. Bachche et al., "Laboratory-based X-ray phase-imaging scanner using Talbot–Lau interferometer for non-destructive testing," *Sci. Rep.* **7**, 6711 (2017).
7. A. Momose et al., "Demonstration of X-ray Talbot interferometry," *Jpn. J. Appl. Phys.* **42**, L866–L868 (2003).
8. T. Weitkamp et al., "X-ray phase imaging with a grating interferometer," *Opt. Express* **13**(16), 6296–6304 (2005).
9. P. Meyer and J. Schulz, "Deep X-ray lithography," in *Micro-Manufacturing Engineering and Technology*, Y. Qin Ed., 2nd ed., pp. 365–391, Elsevier, Boston, Massachusetts (2015).
10. Z. Shi et al., "Towards the fabrication of high-aspect-ratio silicon gratings by deep reactive ion etching," *Micromachines* **11**(9), 864 (2020).
11. K. Jefimovs et al., "High-aspect ratio silicon structures by displacement Talbot lithography and Bosch etching," *Proc. SPIE* **10146**, 101460L (2017).
12. L. Romano and M. Stampanoni, "Microfabrication of x-ray optics by metal assisted chemical etching: a review," *Micromachines* **11**(6), 589 (2020).
13. Z. Shi et al., "Laboratory x-ray interferometry imaging with a fan-shaped source grating," *Opt. Lett.* **46**, 3693–3696 (2021).
14. Z. Shi et al., "High aspect ratio tilted gratings through local electric field modulation in plasma etching," *Appl. Surf. Sci.* **588**, 152938 (2022).
15. S. Pinzek et al., "Fabrication of X-ray absorption gratings via deep X-ray lithography using a conventional x-ray tube," *J. Micro/Nanopatterning, Mater. Metrol.* **20**(4), 043801 (2021).
16. T. Thüring et al., "X-ray phase-contrast imaging at 100 kev on a conventional source," *Sci. Rep.* **4**, 5198 (2014).
17. F. Koch et al., "Note: gratings on low absorbing substrates for X-ray phase contrast imaging," *Rev. Sci. Instrum.* **86**(12), 126114 (2015).
18. P. Meyer and F.-J. Pantenburg, "A Monte Carlo study of the primary absorbed energy redistribution in x-ray lithography," *Microsyst. Technol.* **20**, 1881–1889 (2014).

19. "Advanced technical ceramics mechanical properties of monolithic ceramics at room temperature part 1: Determination of flexural strength," DOD Instruction 1000.01, Standard EN843-1:2007 (2007).
20. Ohio Carbon, "Ohio carbon black graphite and EDM accessories," http://www.ohiocarbonblank.com/index.php?file=graphitematerial_Distdetailurl=edm-af5.
21. T. Koehler et al., "Stable top-bridge manufacturing for dax gratings," European patent application EP 3 786 981 A1 (2021).

Biographies of the authors are not available.